The University of Tehran Press

Pollution

Print ISSN: 2383-451X
Online ISSN: 2383-4501

https://jpoll.ut.ac.ir/

Facile Aqueous Synthesis of Pt-Doped CdTe QDs as Fluorescent Probes for Warfarin Detection in Human Plasma and Urine Samples

Mohsen Samimi[1]✉ | Hosna Ehzari[1] | Meysam Safari[2]✉ | Azeezah Yaseen Yousif[3] | Jafar Nouri[4]

1. Department of Chemical Engineering, Faculty of Engineering, Kermanshah University of Technology, Kermanshah, Iran
2. Department of Chemistry, Faculty of Sciences, Yazd University, Yazd, Iran
3. Department of Chemistry, Faculty of Science, Islamic Azad University, Kermanshah Branch, Kermanshah, Iran
4. Department of Environmental Health Engineering, Tehran University of Medical Sciences, Tehran, Iran

Article Info

Article type:
Research Article

Article history:
Received: 29 March 2024
Revised: 10 May 2024
Accepted: 28 May 2024

Keywords:
Fluorescence red shift
Pt
CdTe
Quantum dots
Quenching
Warfarin detection

ABSTRACT

The existence of warfarin is beneficial for health, but its increase in the human body causes toxicity and increases the risk of bleeding. This research focuses on introducing a facile and safe fluorescence sensor for warfarin detection in biological samples. The synthesis of the fluorescence sensor probe was easily performed with doping metal ions of the Pt to CdTe quantum dots. The morphological and optical properties of the synthesized Pt:CdTe quantum dots were characterized by FT-IR, TEM, and EDX. The interaction patterns of warfarin with CdTe QDs were investigated by the quantum chemical method and compared with experimental results. The proposed quantum dots exhibited a blue luminescence with a 28.8% quantum yield. Pt:CdTe QDs were used as the fluorescence probe to assay warfarin. This procedure is based on the "off" fluorescence of quantum dots in the presence of different concentrations of warfarin. Under optimal conditions, the fluorescence sensor probe could detect the concentration of warfarin with a wide linear range of 0.1–100 µM and a detection limit (S/N = 3) of 0.05 µM. Results of sample analysis by fluorescent nanoprobe displayed that this probe could be the potential alternative tool for warfarin detection in biological samples.

Cite this article: Samimi, M., Ehzari, H., Safari, M., Yaseen Yousif, A., & Nouri, J. (2024). Facile Aqueous Synthesis of Pt-Doped CdTe QDs as Fluorescent Probes for Warfarin Detection in Human Plasma and Urine Samples . *Pollution*, 10 (3), 847-861.
https://doi.org/10.22059/poll.2024.374580.2318

DOI: https://doi.org/10.22059/poll.2024.374580.2318

INTRODUCTION

Protecting human health is one of the constant concerns of humanity (Kasim et al., 2023; Mohadesi et al., 2024; Saeid & Mohammadkhani Orouji, 2023; Samimi & Nouri, 2023; Samimi & Shahriari Moghadam, 2018, 2020). Blood clots in the body can result in serious health complications (Khamooshi et al., 2023; Milani Fard & Milani Fard, 2022). Warfarin is an oral anticoagulant drug derived from coumarin that is widely operated to prevent and treat venous and arterial thromboembolic disorders (Falkenhagen et al., 2023). Warfarin (4-hydroxy-3-(3-oxo-1-phenylbutyl) chromen-2-one) inhibits coagulation factors that require vitamin K to function by inhibiting vitamin K activity (Connolly et al., 2009). This will reduce the amount of material needed to maintain the fibrin filaments in subsequent processes. These events decrease the probability of clot formation, bruising or aching toes, sore throat, fever, chills, swelling of the feet and legs, fatigue, abnormal weight gain, extensive non-traumatic bruising, nasal bleeding,

*Corresponding Author Email: *m.samimi@kut.ac.ir*
m.safary85@gmail.com

and severe and abnormal bleeding from cuts (Shaik et al., 2016). Overdose of warfarin can dilate blood, tear sensitive capillaries, and fill the head with blood, leading to death (Myers et al., 2017; Zemrak et al., 2016). Warfarin interacts with many foods such as lettuce, cucumber, vegetable oil, and medicines such as aspirin - non-steroidal anti-inflammatory drugs (Desai et al., 2017; Ram et al., 2019). Intoxication can be effectively treated with warfarin if the plasma concentration is known. Different analytical techniques including high-performance liquid chromatography (Li et al., 2018) with ultraviolet detection, liquid chromatography-tandem mass spectrometry (Shakleya et al., 2019), Transmission Raman Spectroscopy (Griffen et al., 2018), Thin-Layer Chromatography (de Bairros et al., 2019), Capillary Zone Electrophoresis (Nowak et al., 2015) and Differential Pulse Voltammetry (Chang et al., 2019) have been noted for measuring of warfarin in the biological samples.

The gradual pretreatment steps of the experimental and the high cost of examinations by mentioned procedures have caused them not to be proper for normal analysis. Hence, choosing a substitute procedure with lower operating costs and effective detection speed for assessing the low level of warfarin is an important challenge. According to this view, the use of fluorescence spectroscopy, as a hopeful procedure, was offered for considerable diagnosis in environmental, biochemical and clinical evaluations, etc. (Benson et al., 2023; Cahyonugroho et al., 2022; Ehzari, Amiri, et al., 2022; Ehzari et al., 2021; Ibrahim et al., 2023; Mousavi Ghahfarokhi et al., 2022; Ruf et al., 2019; Samimi & Safari, 2022; Samimi & Validov, 2018). Quantum dots are one of the most studied fluorescence sensors in the field of the biological assay (Cheraghipoor et al., 2024; Ehzari, Safari, et al., 2022; Safari Fard & davoudabadi farahani, 2022). The semiconductor quantum dots are a class of nanocrystal that has received significant interest owing to their unique properties, including narrow emission, excitation spectra, immense size-tunable photophysical, electrical and high quantum yield, etc. (Baharinikoo et al., 2020; Ehzari & Safari, 2022). These fascinating properties of QDs make have been widely applied in a variety of fields such as constructing ratiometric fluorescence sensors, quantitative detection of drugs and bio-imaging (Tan et al., 2020), light sources optoelectronic devices (Jin et al., 2019), and solar cells (Ramanujam et al., 2019). As CdTe QDs contain toxic heavy metal cadmium (Al-Azzawi & Saleh, 2023; Mohammad et al., 2023; Samimi, 2024; Sulistyowati et al., 2023), they are not compatible with biomedical applications (Liu et al., 2022; Noori & Abdulameer, 2022). Doping with proper element is widely used as an effective method to tune surface states, energy levels, and electrical, optical, structural and magnetic properties of semiconducting materials (Ahmadlouydarab et al., 2023; Aldokheily et al., 2022; Islam et al., 2022; Mohsin & Ali, 2023). The critical role that dopants play in semiconductor devices has stimulated research on the properties and the potential applications of semiconductor nanocrystals, or colloidal quantum dots, doped with intentional impurities (Hamid Abd & Adnan Ibrahim, 2022; Hashim & Ibrahim, 2023). The use of intentional impurities, or dopants, to control the behavior of materials lies at the heart of many technologies. For this reason, researchers have begun to explore how dopants can influence semiconductor nanocrystals, crystallites a few nanometers in scale with unusual and size-specific optical and electronic behavior. The energy from absorbed photons can be efficiently transferred to the impurity, quickly localizing the excitation and suppressing undesirable reactions on the nanocrystal surface.Newly, transition metal ions doped quantum dots (d- dots) have been investigated. Doped QDs have added benefits such as less toxicity, longer excited-state lifetimes, wider stokes shifts, improved stability, and high quantum efficiency. (Liu et al., 2019). So far, various transition-metal ions have been doped into II–VI QDs with different impurities, including Co^{2+}, Ni^{2+}, Au^{3+}, Zn^{2+}, Ag^{+}, Pd^{3+}, and Mn^{2+} (Chen et al., 2023; Najafi et al., 2019). Heavy metals are toxic and dangerous in large amounts (Samimi & Amiri, 2024; Samimi & Mansouri, 2024; Samimi & Moeini, 2020; Samimi & Shahriari-Moghadam, 2021; Samimi et al., 2023; Shayegan et al., 2022). Doped QDs can reduce the toxic cadmium ratio in undoped QDs, improving their biological applicability (Najafi et al., 2019). In this work, a simple flu-

orescence nanoprobe was presented by doping Pt to CdTe and thioglycolic acid (TGA) as the stabilizing reagent. The developed nanoprobe has many advantages, including high sensitivity, simplicity, little interference, low toxicity, and accurate measuring result. The Pt:CdTe quantum dots (Pt:CdTe QDs) were synthesized by the hydrothermal method. The photoluminescence characteristics and morphology of the synthesized Pt:CdTe QDs were investigated and then applied as a nanoprobe for the highly sensitive detection of warfarin in plasma samples. The effects of various parameters on the analytical performance were also optimized. Moreover, the probable fluorescence quenching mechanism of Pt:CdTe QDs induced by warfarin is also investigated.

EXPERIMENTAL SUBSTANCES

Cadmium chloride, sodium chloride, sodium borohydride, $H_2PtCl_6 \cdot 6H_2O$, and tellurium powder were prepared from Merck (Darmstadt, Germany). Warfarin and TGA were purchased from Sigma Aldrich (St. Louis, MO, USA). Other routine chemicals were analytical grade purity and were obtained from Merck (Darmstadt, Germany). In addition, Tris–HCl (Tris(hydroxymethyl)aminomethane hydrochloride) buffer solutions (1 mM) at various pH values were prepared. Sodium hydroxide (NaOH) and hydrochloric acid (HCl) solutions have been used the adjustment of the buffer solution's pH (Khorram et al., 2015).

Measurements

The fluorescence quenching measurements were performed with Perkin Elmer (LS55) spectrofluorometer (Ogunsipe, 2018). QDs have excitation and emission wavelengths of 500 and 620 nm, respectively. For all experiments, the slit widths and scan rates were kept constant at 10 nm and 500 nm/min, respectively. Before measurements, samples were purged with pure nitrogen. The measurements were performed using quartz cells ($4 \times 1 \times 1 cm$) with high vacuum Teflon stopcocks. The absorption spectra were measured with a JASCO V630 UV–Visible spectrophotometer. The IR spectra were recorded using a Fourier transform infrared (FTIR) from Thermo Scientific Nicolet IR100 (Madison, WI, USA, ranges of 4000 to 400 cm^{-1}). The crystalline structure, shape, and size of the nanoparticles were evaluated using X-ray diffraction (XRD) (Moulato et al., 2023). The XRD was measured using a PAN analytical X' Pert Pro MPD X-ray diffractometer by Cu Ka radiation k = 0.154 nm with a Ni filter. The tube voltage was 40 k with a tube current of 30 mA.

Computational method

The computational models of warfarin, CdTe-TGA, Pt:CdTe-TGA, as well as CdTe-TGA/warfarin and Pt:CdTe-TGA/warfarin, have been drawn and geometrically optimized by applying Merck Molecular Force Field (MMFF94) in wave function Spartan 16' package (Mousavi et al., 2019). Following, the use of single-point calculation by applying the parameterized hybrid of ab-initio (restricted Hartree-Fock) and semi-empirical quantum mechanical (QM) method (RHF/PM6) has revealed the optical energy diagram of the corresponding models.

Synthesis of Pt:CdTe quantum dots

The previous procedure was used to synthesize Pt:CdTe NPs (Najafi et al., 2018). Briefly, the first step in preparing sodium hydrogen telluride (NaHTe) was to reduce Te powder with $NaBH_4$ in deionized water under stirring conditions and purging with N_2.

The freshly prepared NaHTe nanoparticle was obtained after 3 h. Another flask was prepared by dissolving 0.15 g of $CdCl_2$ and 500 µL of $H_2PtCl_6 \cdot 6H_2O$ (1mM) in 40 ml ultrapure water and adding 200 µl of TGA under stirring conditions and adjusting its pH to 10 by adding dropwise of NaOH solution (1 M) under N_2 purging. Both solutions of free oxygen were mixed and

placed in a Teflon-lined stainless steel autoclave, which was heated in an oven at 120 °C for 3 h. The prepared TGA-coated Pt:CdTe QDs precipitation was washed several times with ethanol after the reaction to remove the excess contaminants.

Preparation of the real samples

Fresh human serum samples were taken from the hospital. 1.5 mL of methanol was added to 3 mL serum; after vortexing of the serum sample for 15 min by centrifugation, the precipitated proteins were separated at 1500 rpm for 20 min. The clear supernatant layer filtrated through a 0.45 mm filter to obtain protein human serum sample and diluted 5 times using twice distilled water while its volume was adjusted to 10 mL. Then, the sample was checked for the determination of the recovery after spiking with known concentrations of warfarin.

Determination of warfarin in urine: 1 mL of a fresh urine sample (healthy human) was filtrated and then with Tris–HCl buffer diluted to 10 mL, 3 mL of this solution was mixed with 100 µL Pt:CdTe QDs (1.0×10-3 mol. L^{-1}) and warfarin, after incubation for 2 min, the FL spectra of the solution were recorded.

Fluorescence measurements

Warfarin with different concentrations (0.1–100 µM) was added to 2 mL of a solution, containing Pt: CdTe QDs (0.1 mg L^{-1}) in 1mM of Tris–HCl buffer solution at pH = 7.5. After 3 min, the fluorescence spectra were recorded at excitation and emission wavelengths of 330 and 557 nm respectively at room temperature. All the spectrofluorometric experiments were measured from 490 nm to 630 nm.

Cell viability assays

The cytotoxicity of Pt: CdTe QDs on fibroblast cells was evaluated by using the activity of the lactate dehydrogenase (LDH) method and reported by Linford with some minor changes. In this study, the primary culture of human fibroblast was used as a normal cell that is derived from the human skin. The cells were seeded in 25 cm^2 tissue culture flasks and maintained in Dulbecco's MEM supplemented with inactivated fetal bovine serum 10%, penicillin 100 U mL^{-1} and streptomycin 100 µg mL^{-1} for 48 h at 37 °C and 5% pCO_2.

The cells (in culture medium) were dispensed in 5×103 per well in 96-well microplates and allowed to incubate overnight. After 24 h of early cell culture, the fresh medium with NPs at concentrations (1.0, 1.5, 2.0, 2.5, 3.0 µM) was renewed. Again, 100 µL of the media from each well was then transferred to new 96-well plates and 100 µL of LDH stock was added to each well and cells were incubated at 37 °C for 30 min. Triton 1% was used as a positive control for the extraction test. The LDH release was estimated using a microplate reader at 495 nm according to the manufacturer's instructions. All measurements were done in triplicate and the mean cell viability was expressed as a percentage of the control.

RESULTS AND DISCUSSION

Chemical and morphology analysis of synthesized Pt:CdTe QDs

The UV–Visible absorption and fluorescence spectra of Pt:CdTe QDs were obtained at 25 ℃ . The absorption spectrum of nanoparticles was measured with the excitonic at 525 nm and it's a wide spectrum. As seen in Fig. 1, the QDs fluorescence were emitted at 563 nm upon excitation at 330 nm. The Pt:CdTe QDs emit near their absorption onset, indicating that the emission is caused by the direct recombination of charge carriers between conduction and valence bands.

The quantum yield (QY) of Pt:CdTe QDs was determined at 28.8 %. QY was attained using the comparative approach by applying quinine sulfate (QY=0.546 in 1M H_2SO_4) as a fluorophore standard at an excitation wavelength of 360 nm. The quantum yield of the Pt:CdTe QDs

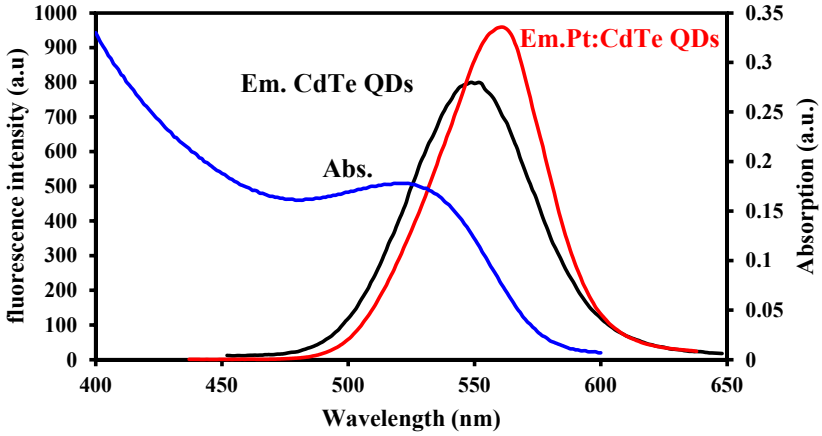

Fig. 1. Normalized UV–Visible absorption and emission spectra of Pt:CdTe QDs.

was increased by 2.1% toward undoped CdTe. Fluorescence emission peaks comparison of QDs shows that the red-shift phenomenon has occurred in the Pt:CdTe QDs. This indicates that platinum has successfully doped into the Pt: CdTe QDs structure. The particle size of Pt: CdTe QDs can be obtained from Eq.1

$$D = [9.8127\exp(-7)]\lambda^3 - [1.7147\exp(-3)]\lambda^2 + 1.0064\lambda - 194.84 \quad (1)$$

The particle size value at the absorption maximum of 525 nm was obtained at around 2.89 nm, which has in good agreement with the TEM observation results.

The concentrations of synthesized CdTe QDs were estimated from the UV–Vis spectrum method by Lambert–Beer's law, which is shown in Eq. 2:

$$A = \varepsilon c \ell \quad (2)$$

where 'A' presents the absorbance of excitonic absorption peak for CdTe QDs, 'c' is the concentration, 'ℓ' is the path length of the radiation beam used, and 'ε' is the molar extinction coefficient of CdTe QDs at the first excitonic absorption peak, which was calculated by $\varepsilon = 10043(D)^{2.12}$. D parameter is the QDs particle size. According to Eq. 2, the concentration of the prepared Pt: CdTe QDs is 2 mM.

FT-IR was used to investigate the surface functionalization of TGA and TGA-capped Pt:CdTe (Fig. 2a). A broad and strong peak at 3441 cm^{-1} was observed in the TGA-capped Pt:CdTe QDs spectrum, which is assigned to O-H bond (stretching vibrations), while this peak is not found in TGA. In TGA, the stretching vibrations of the C=O and S-H bonds were observed at 1716 cm^{-1} and 2565 cm^{-1}, respectively, while in the spectrum of TGA-capped Pt: CdTe QDs the first peak was absent and the second peak was shifted to 1578 cm^{-1}. According to these results, TGA was successfully attached onto quantum dots. The morphology and particle size of the TGA-capped Pt:CdTe QDs were evaluated via TEM image. As it shown in Fig. 2b the prepared QDs with nearly spherical morphology have a uniform size with a diameter about 2 nm. EDX analysis (Das et al., 2023) confirmed the elemental composition of the TGA-capped Pt:CdTe QDs (Fig. 2c). Pt, Cd, and Te were detected in the prepared QDs. Due to the small concentration of doping; the sample contains strong atomic elements of Te, Cd, and Pt. The presence of TGA as a capping agent is also indicated by additional signals such as carbon (C), oxygen (O) and sulfur (S). As shown in Fig. 2d, the crystal structure of Pt:CdTe QDs was studied with XRD

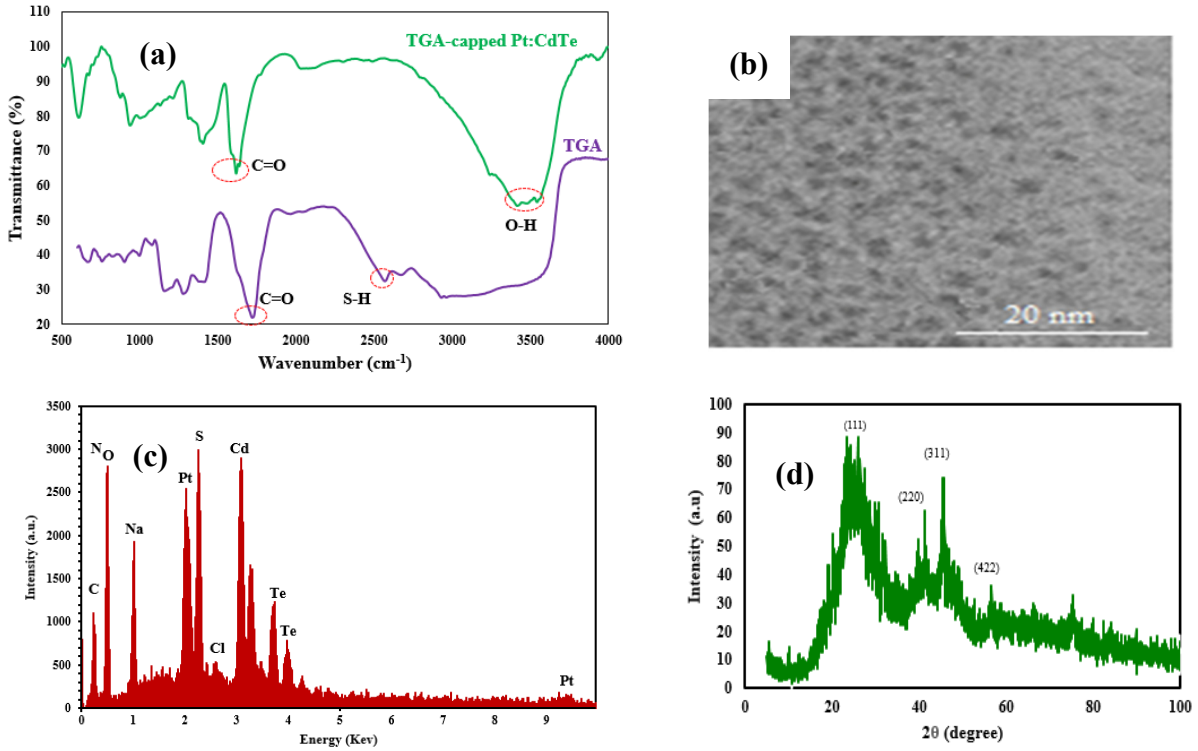

Fig. 2. (a) FT-IR spectrum of Pt:CdTe QDs and TGA (b) TEM image of Pt:CdTe QDs (c) EDX spectrum of Pt:CdTe QDs dried on the glass slide (d) XRD patterns of Pt:CdTe QDs.

pattern (Ibrar et al., 2023). The XRD pattern obtained for the Pt: CdTe QDs indicates four peaks positioned at 2θ = 22.57°, 39.70°, 48.82° and 74.54° that corresponded to (111), (220), (311) and (422) planes. Their positions also are consistent with the values of the standard diffraction patterns of the cubic structure of CdTe (JCPDS no. 03-065-1046).

Optimization of operational conditions

To achieve the maximum performance of the proposed nanoprobe, the operational factors, such as parameters affecting the fluorescence intensity of Pt:CdTe QDs include reaction time and ionic intensity, and pH of solution were optimized. Reaction time is an important factor in fluorescence intensity QDs. So, the QDs were synthesized at different reaction times (0, 60, 90, 120, 180, 240 and 270 min), while the oven temperature was 120 ℃ . With the growth of CdTe QDs, the fluorescence spectrum shifted to longer wavelengths. The maximum emission was observed to react at 120 °C for 180 min. When the reaction time exceeded 180 min, the fluorescence intensity decreased, this may be attributed to the oxidation of the stabilizer molecules, which led to a reduction in the stabilization of the ligands and an increase in surface defects of the QDs (Yu et al., 2012). Stable time Pt:CdTe QDs in an aqueous solution was studied. The fluorescence intensity of Pt:CdTe QDs was stabilized after 70 s. Warfarin reaction time was examined for its effect on the quenching of fluorescence of Pt:CdTe QDs. According to the results, the fluorescence quenching of Pt:CdTe QDs after 2 min was sustained in 10 µM warfarin solution. No change was observed in fluorescence signals of more than 3 min, which indicates that the Pt:CdTe QDs system exhibited good stability. Hence, 2 min equilibration time was chosen for subsequent experiments. NaCl solution was added to evaluate the effect of ionic strength on extraction efficiency. The fluorescence intensities remained constant when NaCl concentrations were 2 %. Therefore, the reaction should take place under low ionic strength conditions. The

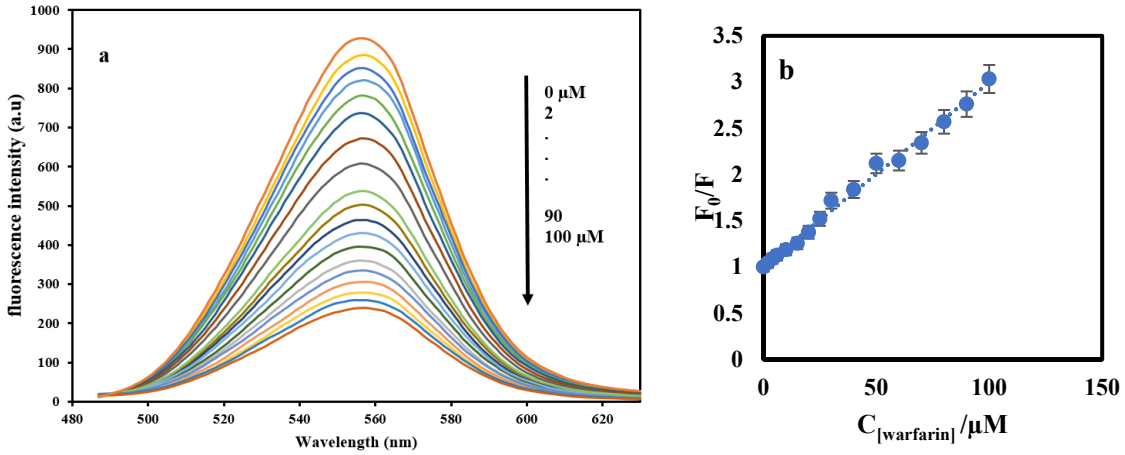

Fig. 3. (a) Fluorescence emission spectrum of the Pt:CdTe QDs (5 µL) in the presence of different warfarin concentrations and (b) the linear relationship of F_0/F versus concentrations of warfarin over the range of 2–100 µM.

pH plays a significant role in the performance of the Pt:CdTe QDs probe. Therefore, the pH effect on the fluorescence intensity in 10 µM of warfarin solution was investigated. Changes ΔI_F vs pH were reported ($\Delta IF = IF^0 - IF$, IF^0 and I_F represent the fluorescence intensities in the presence and absence of warfarin). The maximum fluorescence quenching was observed in pH = 6.0. Therefore, pH of 6.0 was chosen for further experiments. The pH/concentration profiles of warfarin and TGA at a pH of 6.0 show that dominant forms of warfarin are protonated while carboxyl groups of TGA are deprotonated, which indicates that hydrogen bonds play a significant role in the quenching mechanism of TGA-CdTe QDs with warfarin. The Tris-HCl and PBS buffer solutions were used to evaluate the effect of buffer solution on the reaction of Pt:CdTe QDs with drug. To control the acidity interaction of the QDs–warfarin system, a Tris–HCl buffer solution was chosen. The QDs were stored in the dark at 4 °C for evaluating their stability. After 3 months, the fluorescence intensity decreased only to 82.25 % of its initial fluorescence intensity, which shows a good stability.

Analytical performance of the proposed nanoprobe

To study the sensitivity of Pt:CdTe QDs to warfarin, the changes in fluorescence-quenching CdTe quantum dots toward various concentrations warfarin were recorded and the resulted fluorescence spectrogram and its calibration curve are illustrated in Fig. 3. As seen, the fluorescence intensity (F/F_0) decreased gradually with addition of warfarin concentrations, the quenching process of Pt:CdTe QDs with a warfarin could be expressed by the well-known Stern–Volmer equation: $F_0/F = 1 + K_{SV}$ [warfarin]

where, F_0 and F are the fluorescence intensities of the without warfarin and warfarin presence, K_{SV} is the quenching constant. In the range of 0.1 to 100 µM, a calibration curve was obtained with a regression equation of $F_0/F = 1.02 + 0.0482$ [warfarin] and a correlation coefficient (R^2) of 0.9917. The detection limit ($3S_b/m$) was calculated as 0.05 µM, where S_b is the standard deviation of the fluorescence intensity in the absence of warfarin and m is the slope of the calibration curve. The repeatability of the system was also investigated and RSD (for n = 6) of 3.1% in 10 µM warfarin solution was obtained (Table 1).

Selectivity of the proposed nanoprobe

The selective behavior of the fluorescence chemical sensor is one of its most important features. To evaluate the selectivity of the Pt:CdTe QDs for warfarin, the fluorescence response

Table 1. The linear ranges, detection limits and correlation coefficients.

Drug	linear range (μM)	Detection limits (μM)	RSD (%)	Correlation coefficients
Warfarin	0.1-100	0.05	3.1	0.9917

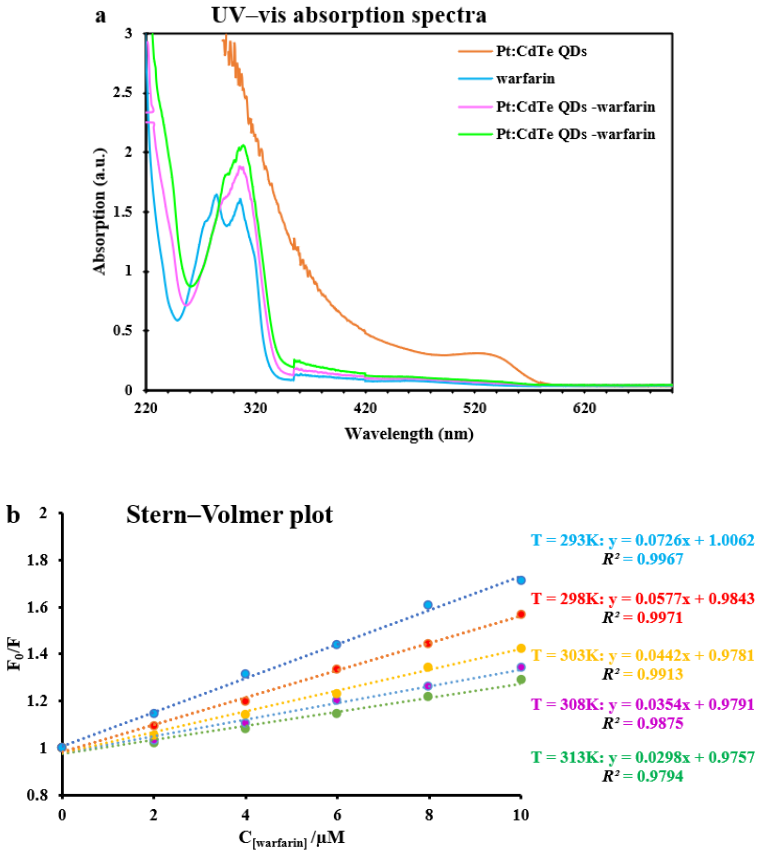

Fig. 4. a) UV–visible absorption spectra of aqueous solution 3.0 mM Pt:CdTe QDs (5 μL) and 10 μM warfarin. b) Stern–Volmer curves for the Pt:CdTe QDs solution system at different temperatures.

by the Pt:CdTe QDs in the presence of the foreign substances, which can be found in human serum, was recorded. The tolerance limit for external substances was determined as the maximum concentration of various substances that gave a relative error less than ±5.0% in presence of 10 μM of warfarin. The results revealed the presence of glucose, glycine, vitamin K, vitamin C, ibuprofen, naproxen and NaCl, KNO_3. The interference results indicate no effect on the fluorescence intensity of Pt:CdTe QDs.

Suggested mechanism of nanoprobe with warfarin

Generally, the quenching process usually occurs through the dynamic quenching or collisional process and the static quenching, which can be confirmed quenching process by UV-vis absorption spectra of QDs in the presence/absence of quencher. In the present work, the Pt:CdTe QDs was stabilized by thioglycolic acid. After adding warfarin to Pt:CdTe QDs solutions, the surface of Pt:CdTe QDs might be changed and cause the increase of surface defects. Warfarin is a drug that has weak acidity (with a pKa of 5.19). Biologically, it acts as a diprotic acid or acid urate ion. As can be seen in Fig. 4a, the structure of warfarin is containing a –OH and C=O, that the –OH and C=O are the key role in the fluorescence quenching of TGA-Pt:CdTe QDs.

Table 2. Determination of warfarin in human plasma and urine samples (n = 3).

Sample	Added (µM)	Total found (n=3)	R.S.D (%)	Recovery (%)
Plasma sample	0	n.d[a]	2.1	0
	20.0	21.0	1.7	105.0
	30.0	29.7	1.6	99.3
Urine sample	0	n.d[a]	1.9	0
	20.0	19.3	2.0	96.6
	40.0	41.6	1.8	104.0

This could lead to hydrogen bonds forming or electrostatic attraction between warfarin and thioglycolic acid coated on the Pt:CdTe QDs and results in an increase in electron localization in the QDs due to the compression of the electron wave function. The Stern-Volmer plots of the quenching of Pt:CdTe QDs by warfarin at various temperatures are shown in Fig. 4b. According to the results, the corresponding Ksv at 293, 298 and 303 K are 3.68, 3.04, 1.99 and 107 L/mol, respectively. To investigate the interaction mechanism between Pt:CdTe QDs and warfarin, the UV-visible absorption spectra of the Pt:CdTe QDs were evaluated in the presence/absence of warfarin. As illustrated in Fig. 4a, when warfarin added to the prepared Pt:CdTe QDs solution, the UV–vis absorption spectra showed an apparent increase in the absorption peak centered at 307 nm, while the absorption peak of the Pt:CdTe QDs decreased at 525 nm. This is indicates that warfarin is coordinated with Pt:CdTe QDs. The absorption spectral change is an important symbol of static fluorescence quenching.

Analysis of real samples

To evaluate the applicability of the proposed fluorescence probe, a certain amount of warfarin was spiked in human plasma and urine samples, respectively. Then the warfarin samples were detected by a standard addition method. The analytical results summarized in Table 2. The result indicated the recoveries were between 96.6% and 105%, suggesting the acceptable accuracy of the proposed nanoprobe for warfarin detection. The accuracy of the proposed procedure was assessed using calculating the relative standard deviations (RSDs). RSDs were achieved in the range from 1.6 to 2.1 %, which reveals the suitable precision of the method for drug monitoring via the proposed fluorescence probe.

Theoretical studies of Pt:CdTe QDs

The interaction of CdTe-TGA QDs with warfarin was evaluated by quantum mechanical (QM) calculations (Fig. 5). As a QD basis, a typical tetrahedral CdTe model with ten Cd and twenty Te atoms was used (Fig. 5B). The Cd-Te bond in this structure has calculated to be 2.77 Å and the net binding energy of -14819.51 kJ mol^{-1} has achieved for the CdTe model. The structure of Pt-doped CdTe QD is shown in Fig. 5C, where one Cd atom at the top of the QD model has replaced with one Pt atom, leading to the Pt-Te bond length of 2.74 Å and the net binding energy of -15718.61 kJ mol^{-1}. This has also widened the bandgap of the QD model up to 2.66 eV. Table 1 shows the computational data of the corresponding models consisting of the binding energy, the energy of the highest occupied molecular orbital (HOMO), the lowest unoccupied molecular orbital (LUMO), and the bandgap. In Fig. 5D and E, the TGA segments are linked to the CdTe and Pt:CdTe QD models through Cd-S and Pt-S covalent bonds with lengths of 2.43 Å and 2.40 Å, respectively. A glance in Table 3 determines the effect of doping the CdTe-TGA QD with the Pt atom, which widened the related HOMO-LUMO gap up to 0.21 eV, suggesting a red-shift in the maximum absorption peak of the UV-Vis spectrum for the Pt-doped QD. Finally, the interaction of the warfarin analyte with both CdTe-TGA and Pt:CdTe-TGA models was investigated. According to Fig. 5F and G, the oxygen-containing functional groups of the

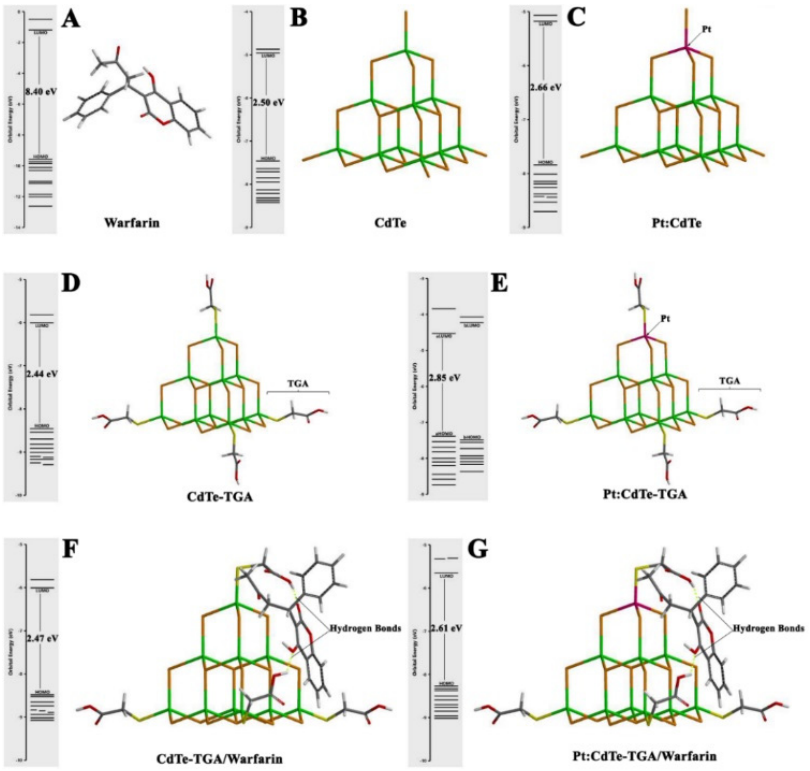

Fig. 5. The geometrically optimized structures and molecular orbital energy diagrams of (A) Warfarin, (B) CdTe, (C) Pt:CdTe, (D) CdTe-TGA, (E) Pt:CdTe-TGA, (F) CdTe-TGA/Warfarin, and (G) Pt:CdTe-TGA/Warfarin models.

Table 3. The results of semi-empirical computational calculations.

No.	Compound	Binding Energy/kJ mol^{-1}	E_{HOMO}/eV	E_{LUMO}/eV	Bandgap/eV
1	Warfarin	-435.98	-9.58	-1.18	8.40
2	CdTe	-14819.51	-7.46	-4.96	2.50
3	Pt:CdTe	-15718.61	-7.84	-5.18	2.66
4	CdTe-TGA	-15936.93	-8.45	-6.01	2.44
5	Pt:CdTe-TGA	-16348.51	-7.38	-4.53	2.85
6	CdTe-TGA/Warfarin	-14300.77	-8.48	-6.01	2.47
7	Pt:CdTe-TGA/Warfarin	-14650.54	-8.27	-5.66	2.61

warfarin molecules have attracted to the TGA segments of the corresponding QDs through hydrogen bonds. In terms of the optical interaction between QD and warfarin, the role of Pt dopant in the QD structure become more significant since the interaction of Pt:CdTe-TGA QD with warfarin has *ca.*350 kJ mol^{-1} lower binding energy (i.e. more stable interaction) compared to CdTe-TGA and resulted in wider bandgap equals to 0.14 eV. This phenomenon can also provide a red shift in the UV-Vis spectrum of Pt:CdTe-TGA/Warfarin versus CdTe-TGA/Warfarin.

Cytotoxicity Analysis

To measure the activity of Pt: CdTe QDs on the fibroblast cells, LDH assay was accomplished (Fig. 6). It was found that the Pt: CdTe QDs exhibit dose-dependent cytotoxicity. However, this result reveals that the nanoparticles have notable toxicity at 3.0 µM, but, after treatment with the lower concentration of Pt: CdTe QDs (i.e. 1.0, 1.5, 2.0, and 2.5 µM) for 48 h, no cytotoxicity effects were observed. Nevertheless, the dosage used for experiments is much smaller than this concentration which does not have toxic effects.

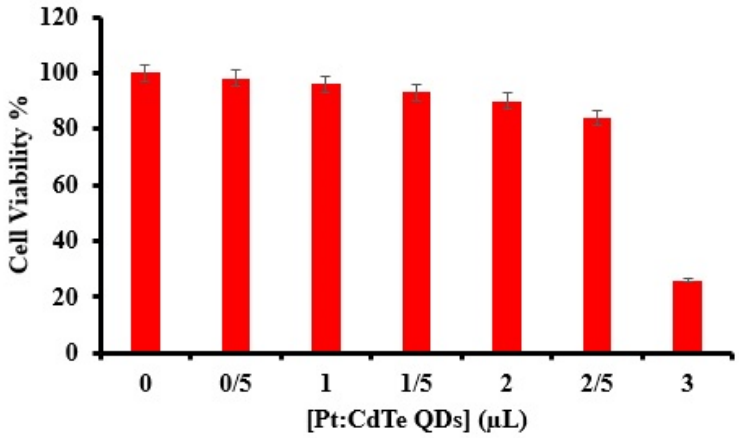

Fig. 6. Cell viability of fibroblast cells mixed with the different concentration of Pt: CdTe QDs for 48 h at 37 °C.

CONCLUSIONS

In this work, the Pt: CdTe QDs synthesized and fully characterized by hydrothermal synthesis. The Pt: CdTe QDs utilized as ratiometric fluorescent sensor for highly selective and sensitive the warfarin in human plasma and urine. The fluorescent sensor was constructed based on the quenching effect of proposed nannoprobe during the reaction with warfarin in rang 0.1 to 100 µM. The advantages of this nanoprobe include facile synthesis, no expensive materials, rapidity, simplicity, and high sensitivity. The presented sensor displayed promising opportunities for the quantitative determination of warfarin drug in medical clinics.

GRANT SUPPORT DETAILS

The present research did not receive any financial support.

CONFLICT OF INTEREST

The authors declare that there is not any conflict of interests regarding the publication of this manuscript. In addition, the ethical issues, including plagiarism, informed consent, misconduct, data fabrication and/ or falsification, double publication and/ or submission, and redundancy has been completely observed by the authors.

LIFE SCIENCE REPORTING

No life science threat was practiced in this research.

REFERENCES

Ahmadlouydarab, M., Javadi, S., & Adel Alijan Darab, F. (2023). Evaluation of Thermal Stability of TiO2 Applied on the Surface of a Ceramic Tile to Eliminate Methylene Blue Using Silica-based Doping Materials. *Advanced Journal of Chemistry, Section A, 6*(4), 352-365.

Al-Azzawi, M., & Saleh, W. (2023). Fabrication of environmental monitoring amperometric biosensor based on alkaloids compound derived from catharanthus roseus extract nanoparticles for detection of cadmium pollution of water. *Chem. Methodol., 7*(5), 358-371.

Aldokheily, M. E., Mekky, A. H., & Rahem, S. A. (2022). Preparation of Polymer Nanoparticles and Doping by Some Schiff Base Compounds by using Microemulsion Systems. *Chemical Methodologies, 6*(6), 494-500.

Baharinikoo, L., Chaichi, M., & Ganjali, M. (2020). Detecting the quantity of acrylamide in potato chips utilizing CdTe surface functionalized quantum dots with fluorescence spectroscopy. *International Journal of Peptide Research and Therapeutics, 26*(2), 823-830.

Benson, A., Akinterinwa, A., Milam, C., & Hammed, A. M. (2023). Chemical Profiling of Minerals and Elemental Composition of Rock and Soil Samples from Bakin Dutse Hills, Madagali, Adamawa State Nigeria. *Eurasian Journal of Science and Technology, 3*(4), 232-245.

Cahyonugroho, O. H., Hariyanto, S., & Supriyanto, G. (2022). Dissolved organic matter and its correlation with phytoplankton abundance for monitoring surface water quality. *Global Journal of Environmental Science and Management, 8*(1), 59-74.

Chang, Y.-T., Wang, Z.-R., & Hsieh, M.-M. (2019). Sensitive determination of warfarin and its metabolic enantiomers in body fluids via capillary electrophoresis combined with ultrasound-assisted dispersive liquid-liquid microextraction and online sample stacking. *Microchemical Journal, 146*, 1276-1284.

Chen, X., Liu, Y., Zhong, M., Yang, J., Lin, Z., & Liang, Y. (2023, 2023/01/01). Preparation and properties of boron affinity molecularly imprinted mesoporous polymers based on Mn-doped ZnS quantum dots. *Analytical Sciences, 39*(1), 13-22.

Cheraghipoor, M., Zakeri, M., Moghadam, H., & Samimi, M. (2024). A Feasibility Study for the Preparation of Green Copper-Colored Mica Pearlescent Pigments. *Advanced Journal of Chemistry, Section A, 7*(3), 338-346.

Connolly, S. J., Ezekowitz, M. D., Yusuf, S., Eikelboom, J., Oldgren, J., Parekh, A., Pogue, J., Reilly, P. A., Themeles, E., & Varrone, J. (2009). Dabigatran versus warfarin in patients with atrial fibrillation. *New England Journal of Medicine, 361*(12), 1139-1151.

Das, R., Mukherjee, D., Reja, S., Sarkar, K., & Kejriwal, A. (2023). Copper Based N,N-Dimethyl-N-(1-Pyridinylmethylidene) Propane-1,3-Diamine Compound: Synthesis, Characterization, and Its Application toward Biocidal Activity. *Journal of Applied Organometallic Chemistry, 3*(2), 73-85.

de Bairros, A. V., Dias, D., Bezerra, A., Wagner, R., Klein, B., Kommers, G., Stefanon, E., & Pego, A. M. (2019). An analytical strategy for the identification of carbamates, toxic alkaloids, phenobarbital and warfarin in stomach contents from suspected poisoned animals by thin-layer chromatography/ultraviolet detection. *Toxicology mechanisms and methods*(just-accepted), 1-38.

Desai, A., Yamazaki, T., Dietz, A. J., Kowalski, D., Lademacher, C., Pearlman, H., Akhtar, S., & Townsend, R. (2017). Pharmacokinetic and pharmacodynamic evaluation of the drug-drug interaction between isavuconazole and warfarin in healthy subjects. *Clinical pharmacology in drug development, 6*(1), 86-92.

Ehzari, H., Amiri, M., Safari, M., & Samimi, M. (2022). Zn-based metal-organic frameworks and p-aminobenzoic acid for electrochemical sensing of copper ions in milk and milk powder samples. *International Journal of Environmental Analytical Chemistry, 102*(16), 4364-4377.

Ehzari, H., & Safari, M. (2022). A Sandwich-Type Electrochemical Immunosensor Using Antibody-Conjugated Pt-Doped CdTe QDs as Enzyme-Free Labels for Sensitive HER2 Detection Based on a Magnetic Framework. *Frontiers in Chemistry, 10*, 881960.

Ehzari, H., Safari, M., & Samimi, M. (2021). Signal amplification of novel sandwich-type genosensor via catalytic redox-recycling on platform MWCNTs/Fe3O4@ TMU-21 for BRCA1 gene detection. *Talanta, 234*, 122698.

Ehzari, H., Safari, M., Samimi, M., Shamsipur, M., & Gholivand, M. B. (2022). A highly sensitive electrochemical biosensor for chlorpyrifos pesticide detection using the adsorbent nanomatrix contain the human serum albumin and the Pd: CdTe quantum dots. *Microchemical Journal, 179*, 107424.

Falkenhagen, U., Knöchel, J., Kloft, C., & Huisinga, W. (2023). Deriving mechanism-based pharmacodynamic models by reducing quantitative systems pharmacology models: An application to warfarin. *CPT: Pharmacometrics & Systems Pharmacology, 12*(4), 432-443.

Griffen, J. A., Owen, A. W., & Matousek, P. (2018). Quantifying low levels (< 0.5% w/w) of warfarin sodium salts in oral solid dose forms using Transmission Raman spectroscopy. *Journal of pharmaceutical and biomedical analysis, 155*, 276-283.

Hamid Abd, A., & Adnan Ibrahim, O. (2022). Synthesis of Carbon Quantum Dot by Electro-Chemical Method and Studying Optical, Electrical, and Structural Properties. *Chemical Methodologies, 6*(11), 823-830.

Hashim, A. E., & Ibrahim, F. T. (2023). A Novel Design for Gas Sensor of Zinc Oxide Nanostructure Prepared by Hydrothermal Annealing Technique. *Chemical Methodologies, 7*(4), 314-324.

Ibrahim, F. T., Shahoodh, M. A., & Guermazi, S. (2023). Studying the Structural and Optical Properties of Thin Compound Oxide Films Based on TiO2: NiO: In2O3 Nanostructure. *Chemical Methodologies, 7*(11), 871-882.

Ibrar, S., Zafar Ali, N., Ojegu, E. O., Odia, O. B., L. Ikhioya, I., & Ahmad, I. (2023). Assessing High-Performance Energy Storage of the Synthesized ZIF-8 and ZIF-67. *Journal of Applied Organometallic Chemistry, 3*(4), 294-307.

Islam, J., Kumer, A., Chakma, U., Alam, M. M., Biswas, S., Ahmad, Z., Islam, M. S., Jony, M. I. J., & Ahmed, M. B. (2022). Investigation of Structural, Electronic, and Optical Properties of SrTiO3 and SrTi0.94Ag0.06O3 Quantum Dots Based Semiconductor Using First Principle Approach. *Advanced Journal of Chemistry, Section A, 5*(2), 164-174.

Jin, S. H., Choi, J. C., & Lee, H. S. (2019). Temperature-Dependent Photoluminescence in CdTe/ZnTe Triple Quantum Dots. *Journal of the Korean Physical Society, 74*(2), 173-176.

Kasim, S., Daud, A., Birawida, A. B., Mallongi, A., Arundana, A. I., Rasul, A., & Hatta, M. (2023). Analysis of environmental health risks from exposure to polyethylene terephthalate microplastics in refilled drinking water. *Global Journal of Environmental Science and Management, 9*(Special Issue (Eco-Friendly Sustainable Management)), 301-318.

Khamooshi, F., Doraji-Bonjar, S., Akinnawo, A. S., Ghaznavi, H., Salimi-Khorashad, A. R., & Khamooshi, M. J. (2023). Dark Classics in Chemical Neuroscience: Comprehensive Study on the Biochemical Mechanisms and Clinical Implications of Opioid Analgesics. *Chemical Methodologies, 7*(12), 964-993.

Khorram, M., Samimi, M., Samimi, A., & Moghadam, H. (2015). Electrospray preparation of propranolol-loaded alginate beads: Effect of matrix reinforcement on loading and release profile. *Journal of Applied Polymer Science, 132*(4).

Li, W., Bu, F., Li, R., Wang, B., Shaikh, A. S., Zhang, Y., Guo, R., & Zhang, R. (2018). Bioequivalence Study of Warfarin in Healthy Chinese Volunteers With a Validated High-Performance Liquid Chromatography-Mass Spectrometry Method. *Clinical pharmacology in drug development, 7*(3), 256-262.

Liu, J., Zhang, Q., Xue, W., Zhang, H., Bai, Y., Wu, L., Zhai, Z., & Jin, G. (2019). Fluorescence Characteristics of Aqueous Synthesized Tin Oxide Quantum Dots for the Detection of Heavy Metal Ions in Contaminated Water. *Nanomaterials, 9*(9), 1294.

Liu, P., Hao, R., Sun, W., Lin, Z., Jing, T., & Yang, H. (2022, 2022/10/01). A "bottle-around-ship" method to encapsulated carbon nitride and CdTe quantum dots in ZIF-8 as the dual emission fluorescent probe for detection of mercury (II) ion. *Analytical Sciences, 38*(10), 1305-1312.

Milani Fard, M., & Milani Fard, A. M. (2022). Evaluation of Office Stones in Kidney Patients and How to form and Treat Them. *Eurasian Journal of Science and Technology, 2*(2), 115-129.

Mohadesi, M., Gouran, A., Darabi, F., & Samimi, M. (2024). Sunflower seed pulp ash as an efficient and eco-friendly adsorbent for Congo red uptake: characteristics, kinetics, and optimization. *Water Practice & Technology, 19*(1), 228-240.

Mohammad, I. A., Madaki, S. K., Tabugbo, B. I., & Usman, R. (2023). Assessment of Heavy Metals in Soil from Selected Farmlands in Nasarawa West, Nasarawa State, Nigeria. *Journal of Applied Organometallic Chemistry, 3*(3), 245-254.

Mohsin, M. M., & Ali, F. H. (2023). Enhancement of Pigments Hydrophobicity by Mixing with Cr Doped SiO2 Nanoparticles. *Chemical Methodologies, 7*(5), 335-347.

Moulato, K., Ammari, M., & Ben Allal, L. (2023). Performance of sewage sludge reuse in the manufacturing of fired bricks. *Global Journal of Environmental Science and Management, 9*(3), 477-496.

Mousavi, F., Shamsipur, M., Taherpour, A. A., & Pashabadi, A. (2019). A rhodium-decorated carbon nanotube cathode material in the dye-sensitized solar cell: Conversion efficiency reached to 11%. *Electrochimica Acta, 308*, 373-383.

Mousavi Ghahfarokhi, S. E., Helfi, K., & Zargar Shoushtari, M. (2022). Synthesis of the Single-Phase Bismuth Ferrite (BiFeO3) Nanoparticle and Investigation of Their Structural, Magnetic, Optical and Photocatalytic Properties. *Advanced Journal of Chemistry, Section A, 5*(1), 45-58.

Myers, S. P., Dadashzadeh, E. R., Cheung, J., Alarcon, L., Kutcher, M., Brown, J. B., & Neal, M. D. (2017). Management of anticoagulation with rivaroxaban in trauma and acute care surgery: complications and reversal strategies as compared to warfarin therapy. *Journal of Trauma and Acute Care Surgery, 82*(3), 542-549.

Najafi, S., Amani, S., & Shahlaei, M. (2018). Rapid determination of the anti-cancer agent Gemcitabine in biological samples by fluorescence sensor based on Au-doped CdTe. *Journal of Molecular Liquids, 266*, 514-521.

Najafi, S., Safari, M., Amani, S., Mansouri, K., & Shahlaei, M. (2019). Preparation, characterization and cell cytotoxicity of Pd-doped CdTe quantum dots and its application as a sensitive fluorescent nanoprobe. *Journal of Materials Science: Materials in Electronics, 30*(15), 14233-14242.

Noori, H. N., & Abdulameer, A. F. (2022). Study of Optical and Structural Properties of CdTe Quantum Dots Capped with 3MPA Using Hydrothermal Method. *Chemical Methodologies, 6*(11), 842-850.

Nowak, P., Garnysz, M., Mitoraj, M. P., Sagan, F., Woźniakiewicz, M., & Kościelniak, P. (2015). Analytical aspects of achiral and cyclodextrin-mediated capillary electrophoresis of warfarin and its two main derivatives assisted by theoretical modeling. *Journal of Chromatography A, 1377*, 106-113.

Ogunsipe, A. (2018). Semi-empirical Estimation of Rhodamine 6G's Fluorescence Lifetimes from Fluorescence Quenching Data. *Chemical Methodologies, 2*(4), 291-298.

Ram, V. R., Dubal, K. L., Dave, P., & Joshi, H. S. (2019). Development and Validation of a Stability Indicating HPLC Assay Method for Determination of Warfarin Sodium in Tablet Formulation. *Chemical Methodologies, 3*(3), 322-339.

Ramanujam, J., Bishop, D. M., Todorov, T. K., Gunawan, O., Rath, J., Nekovei, R., Artegiani, E., & Romeo, A. (2019). Flexible CIGS, CdTe and a-Si: H based thin film solar cells: A review. *Progress in Materials Science*, 100619.

Ruf, V. C., Nübling, G. S., Willikens, S., Shi, S., Schmidt, F., Levin, J., Bötzel, K., Kamp, F., & Giese, A. (2019). Different effects of α-synuclein mutants on lipid binding and aggregation detected by single molecule fluorescence spectroscopy and ThT fluorescence-based measurements. *ACS chemical neuroscience, 10*(3), 1649-1659.

Saeid, Z., & Mohammadkhani Orouji, F. (2023). Comparing the Effect of Meditation with the Brain. *Eurasian Journal of Science and Technology, 3*(2), 93-103.

Safari Fard, V., & davoudabadi farahani, Y. (2022). An Amine/Imine Functionalized Microporous MOF as a New Fluorescent Probe Exhibiting Selective Sensing of Fe3+ and Al3+ Over Mixed Metal Ions. *Journal of Applied Organometallic Chemistry, 2*(4), 165-179.

Samimi, M. (2024). Efficient biosorption of cadmium by Eucalyptus globulus fruit biomass using process parameters optimization. *Global Journal of Environmental Science and Management, 10*(1), 27-38.

Samimi, M., & Amiri, K. (2024). Zinc Alginate Beads as an Effective Biosorbent for the Removal of Eosin-B from Aquatic Solutions: Equilibrium, Kinetics, and Thermodynamic Behaviors. *Chemical Methodologies*, 351-363.

Samimi, M., & Mansouri, E. (2024). Efficiency evaluation of Falcaria vulgaris biomass in Co (II) uptake from aquatic environments: characteristics, kinetics and optimization of operational variables. *International Journal of Phytoremediation, 26*(4), 493-503.

Samimi, M., & Moeini, S. (2020). Optimization of the Ba+ 2 uptake in the formation process of hydrogels using central composite design: Kinetics and thermodynamic studies of malachite green removal by Ba-alginate particles. *Journal of Particle Science and Technology, 6*(2), 95-102.

Samimi, M., & Nouri, J. (2023). Optimized Zinc Uptake from the Aquatic Environment Using Biomass Derived from Lantana Camara L. Stem. *Pollution, 9*(4), 1925-1934.

Samimi, M., & Safari, M. (2022). TMU-24 (Zn-based MOF) as an advance and recyclable adsorbent for the efficient removal of eosin B: Characterization, equilibrium, and thermodynamic studies. *Environmental Progress & Sustainable Energy*, e13859.

Samimi, M., & Shahriari-Moghadam, M. (2021). Isolation and identification of Delftia lacustris Strain-MS3 as a novel and efficient adsorbent for lead biosorption: Kinetics and thermodynamic studies, optimization of operating variables. *Biochemical Engineering Journal, 173*, 108091.

Samimi, M., & Shahriari Moghadam, M. (2018). Optimal conditions for the biological removal of ammonia from wastewater of a petrochemical plant using the response surface methodology. *Global Journal of Environmental Science and Management, 4*(3), 315-324.

Samimi, M., & Shahriari Moghadam, M. (2020). Phenol biodegradation by bacterial strain O-CH1 isolated from seashore. *Global Journal of Environmental Science and Management, 6*(1), 109-118.

Samimi, M., & Validov, S. (2018). Characteristics of pDNA-loaded chitosan/alginate-dextran sulfate nanoparticles with high transfection efficiency. *Romanian Biotechnological Letters, 23*(5), 13996-14006.

Samimi, M., Zakeri, M., Alobaid, F., & Aghel, B. (2023). A Brief Review of Recent Results in Arsenic Adsorption Process from Aquatic Environments by Metal-Organic Frameworks: Classification Based on Kinetics, Isotherms and Thermodynamics Behaviors. *Nanomaterials, 13*(1), 60.

Shaik, A. N., Bohnert, T., Williams, D. A., Gan, L. L., & LeDuc, B. W. (2016). Mechanism of drug-drug interactions between warfarin and statins. *Journal of pharmaceutical sciences, 105*(6), 1976-1986.

Shakleya, D., Rahman, Z., & Faustino, P. J. (2019). Development and validation of an ultra-high-performance liquid chromatography–tandem mass spectrometry method to determine the bioavailability of warfarin and its major metabolite 7-hydroxy warfarin in rats dosed with oral formulations containing different polymorphic forms. *Biomedical Chromatography, 33*(12), e4685.

Shayegan, H., Safari Fard, V., Taherkhani, H., & Rezvani, M. A. (2022). Efficient Removal of Cobalt(II) Ion from Aqueous Solution Using Amide-Functionalized Metal-Organic Framework. *Journal of Applied Organometallic Chemistry, 2*(3), 109-118.

Sulistyowati, L., Yolanda, Y., & Andareswari, N. (2023). Harbor water pollution by heavy metal concentrations in sediments. *Global Journal of Environmental Science and Management, 9*(4), 885-898.

Tan, X., Li, Q., & Yang, J. (2020). A simple fluorescence method detection levofloxacin in milk based on GSH-CdTe QDs. *Journal of Molecular Structure, 1201*, 127175.

Yu, Y., Xu, L., Chen, J., Gao, H., Wang, S., Fang, J., & Xu, S. (2012). Hydrothermal synthesis of GSH–TGA co-capped CdTe quantum dots and their application in labeling colorectal cancer cells. *Colloids and Surfaces B: Biointerfaces, 95*, 247-253.

Zemrak, W. R., Kelley, E., Kovacic, N. L., Mooney, D. M., Morris, J. G., MacVane, C. Z., & Rosenblatt, J. A. (2016). Thrombotic complications following the administration of high-dose prothrombin complex concentrate for acute warfarin reversal. *The American journal of emergency medicine, 34*(8), 1736. e1731-1736. e1733.